

UT-11-16
IPMU-11-0088

LHC signature with long-lived stau in high reheating temperature scenario

Motoi Endo^{1,2}, Koichi Hamaguchi^{1,2}, Kouhei Nakaji¹¹ *Department of Physics, University of Tokyo, Tokyo 113-0033, Japan*² *Institute for the Physics and Mathematics of the Universe, University of Tokyo,
Chiba 277-8568, Japan*

Abstract

We study the possibility of observing the stau signal at LHC in case that the gravitino is the lightest supersymmetric particle and the stau is the next lightest supersymmetric particle in high reheating temperature scenario. We show that a number of stau signals can be observed at LHC for $\sqrt{s} = 7$ TeV and an integrated luminosity of 1 fb^{-1} in most of the parameter region for the reheating temperature $T_R \gtrsim \mathcal{O}(10^8) \text{ GeV}$. We also show that the parameter region with $T_R \gtrsim 2 \times 10^9 \text{ GeV}$, which is consistent with the thermal leptogenesis, is all covered for $\sqrt{s} = 14$ TeV with 10 fb^{-1} .

1 Introduction

Supersymmetry (SUSY) is one of the most plausible models beyond the standard model. In some classes of minimal supersymmetric standard model (MSSM) with the gravitino, the gravitino (\tilde{G}) becomes the lightest supersymmetric particle (LSP) and the lightest stau ($\tilde{\tau}$) becomes the next-to-lightest supersymmetric particle (NLSP). Such a scenario may predict the stau lifetime longer than $\mathcal{O}(1)$ sec because of the weak coupling between the gravitino and the stau. The existence of the long-lived charged massive particles like the stau is appealing from the viewpoint of the discovery at the collider, since they are observed as charged tracks at the detector. The search for such long-lived particles at LHC has already started [1].

However, there are some cosmological problems in this scenario. The present energy density of the gravitino produced in the thermal scattering at the epoch of reheating may exceed the observed dark matter energy density. Moreover, the existence or the late-time decay of the stau at the epoch of Big Bang Nucleosynthesis (BBN) may spoil the successful BBN. It has been pointed out that, from these two cosmological constraints, upper bounds on the gluino mass are obtained for a given reheating temperature and for a given stau mass [2] (see also [3]). Such upper bounds on the gluino mass predicts promising collider signatures of this long-lived stau scenario.

In this paper, we study the observability of the stau signals at LHC in this long-lived stau scenario under the cosmological constraints, assuming that the R-parity is conserved, and that there is no entropy production after the reheating. We show that a higher reheating temperature predicts a lower gluino mass, and therefore more stau signals can be observed at LHC. It is shown that a number of stau signals can be observed at the early LHC (the center-of-mass energy $\sqrt{s} = 7$ TeV and the integrated luminosity $L_i = 1 \text{ fb}^{-1}$) in most of the parameter region for $T_R \gtrsim \mathcal{O}(10^8)$ GeV. We also show that the parameter region with $T_R \gtrsim 2 \times 10^9$ GeV, which is consistent with the thermal leptogenesis [4, 5], is all covered for $\sqrt{s} = 14$ TeV and $L_i = 10 \text{ fb}^{-1}$. This paper is the complete version of our previous work [6]. In addition to the analysis in our previous paper, we include the followings in this paper. We study the parameter region where the stau annihilates near the pole of CP-even heavy Higgs boson. The upper bounds on the gluino mass are shown in various gaugino mass relations. The results using the detector simulation are shown in more details.

This paper is organized as follows. In Section 2, we discuss the cosmological constraints. In Section 3, the constraints from Tevatron and the signatures at LHC are studied. We conclude this paper in Section 4.

2 Cosmological Constraints

In this section, we discuss the cosmological constraints in the scenario with a long lived stau and with high reheating temperature. There are mainly two constraints: the constraints from gravitino over-production and the constraints from BBN. The over-production bound is reviewed in Sec.2.1, where an upper bound on the gluino mass is obtained for a given gravitino mass and a reheating temperature. In Sec.2.2, we discuss the BBN bound, and we get an upper bound on the gravitino mass for a given stau mass. Combining these two cosmological constraints, an upper bound on the gluino mass is obtained for a given stau mass and a reheating temperature.

We discuss the three different annihilation processes of staus: (i) electroweak processes, (ii) annihilation into light Higgs bosons(h) [7, 8] and (iii) annihilation near the pole of CP-even heavy Higgs boson(H) [8].

2.1 Gravitino Over-production Bound

The gravitinos are produced by the scattering process of particles in thermal bath after the epoch of reheating [9, 10, 11, 12]. The gravitino abundance takes the form of [11]

$$\Omega_{3/2} h^2 \simeq \left(\frac{T_R}{10^8 \text{ GeV}} \right) \left(3.7 \times 10^{-4} \left(\frac{m_{3/2}}{100 \text{ GeV}} \right) + \left(\frac{1 \text{ GeV}}{m_{3/2}} \right) \left[0.14 \left(\frac{m_{\tilde{B}}}{1 \text{ TeV}} \right)^2 + 0.38 \left(\frac{m_{\tilde{W}}}{1 \text{ TeV}} \right)^2 + 0.34 \left(\frac{m_{\tilde{g}}}{1 \text{ TeV}} \right)^2 \right] \right), \quad (1)$$

where $m_{3/2}$, $m_{\tilde{B}}$, $m_{\tilde{W}}$ and $m_{\tilde{g}}$ are the physical masses of the gravitino, the bino, the wino and the gluino respectively. The reheating temperature T_R is defined by

$$T_R = \left(\frac{\pi^2 g_*(T_R)}{90} \right)^{-1/4} \sqrt{\Gamma_\phi M_P}, \quad (2)$$

where Γ_ϕ is the inflaton decay rate, g_* is effective degrees of freedom and $M_P = 2.4 \times 10^{18}$ GeV is the Planck scale. We used the one-loop renormalization group equations to evolve the running masses of gauginos up to the scale $\mu = T_R$. The numerical coefficients, which depend on T_R logarithmically, are evaluated at $T_R = 10^8 \text{ GeV}$ in Eq.(1). In the numerical analysis, we include those logarithmic dependences. Note that Eq.(1) potentially includes an $\mathcal{O}(1)$ uncertainty [10, 12].

Although gravitinos can be also produced by inflaton decay [13] and the moduli decay [14], they are model dependent, and we do not include these production processes, for simplicity.

In the present scenario, late-time stau decay also produces gravitinos,

$$\Omega_{3/2}^{NT} h^2 \simeq 2.8 \times 10^{-7} \left(\frac{Y_{\tilde{\tau}}}{10^{-15}} \right) \left(\frac{m_{3/2}}{1 \text{ GeV}} \right), \quad (3)$$

where $Y_{\tilde{\tau}} \equiv n_{\tilde{\tau}}/s$ is the stau abundance, $n_{\tilde{\tau}} = n_{\tilde{\tau}}^+ + n_{\tilde{\tau}}^-$ is stau number density after the freeze-out, and s is the entropy density. However, its contribution is negligible in the parameter region of our interest, and we neglect it in the following discussion.

The gravitino energy density should not exceed the observed DM density [15],

$$\Omega_{3/2} h^2 \leq 0.122 \text{ (95\% C.L.)}. \quad (4)$$

This constraint gives the upper bound on the value of gluino mass for a given gravitino mass and reheating temperature, for fixed values of bino mass and wino mass. The most conservative bound is obtained for $m_{\tilde{B}} = m_{\tilde{W}} = m_{3/2}$, which is shown in Fig.1. In the lower gravitino mass region, the term proportional to $m_g^2/m_{3/2}$ dominantly contributes to the right-hand side in Eq.(1). Thus, in that region, the upper bound on $m_{\tilde{g}}$ is proportional to $\sqrt{m_{3/2}}$, as we can see in Fig. 1. On the other hand, we see that the upper bounds drop down in the higher gravitino mass region, because the terms proportional to $m_{3/2}$ and $m_{\tilde{B}/\tilde{W}}^2/m_{3/2}$ become non-negligible.

We find that in gravitino LSP scenario, the gluino mass cannot be higher than 2.5 TeV for $T_R \gtrsim 2 \times 10^9$ GeV which is required in the thermal leptogenesis [4, 5]. It is also found that the reheating temperature higher than $\mathcal{O}(10^{10})$ GeV is not allowed in the scenario with gravitino LSP. Note that these bounds are the most conservative ones and should be satisfied independently of the BBN constraints, unless there is an entropy production after the gravitino production.

2.2 BBN Bound

In the present scenario, staus are long-lived so that they may affect BBN. There is an upper bound on the stau lifetime depending on the value of stau relic abundance at the BBN epoch. The stau lifetime is given by

$$\tilde{\tau}_{\tilde{\tau}} = \frac{48\pi M_P^2 m_{3/2}^2}{m_{\tilde{\tau}}^5} \left(1 - \frac{m_{3/2}^2}{m_{\tilde{\tau}}^2} \right)^{-4}, \quad (5)$$

and hence the upper bound on the stau lifetime can be translated into an upper bound on the gravitino mass for a given stau mass.

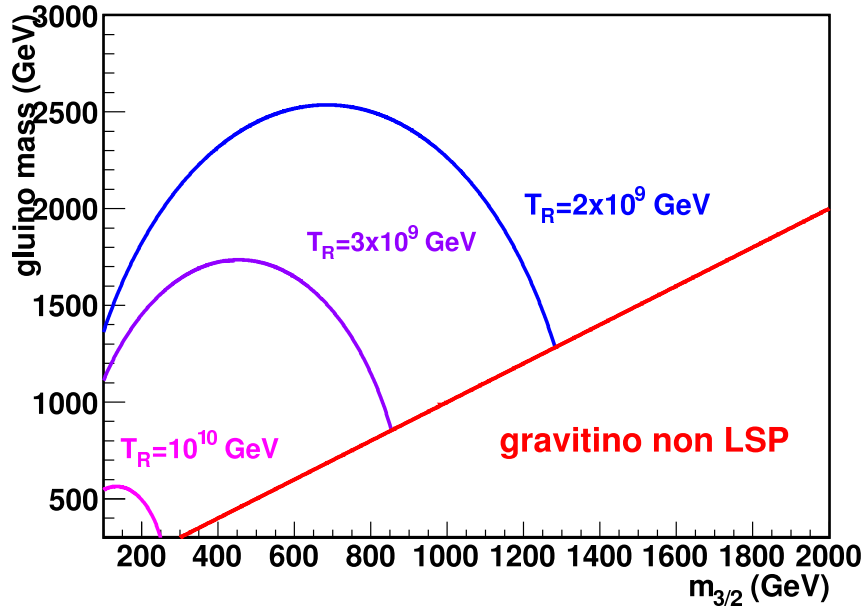


Figure 1: The upper bound on the gluino mass in case that $M_{\tilde{B}} = M_{\tilde{W}} = m_{3/2}$.

Among the constraints on stau lifetime from BBN, the most stringent bound comes from the catalyzed effect where stau forms a bound state with ${}^4\text{He}$ and overproduces ${}^6\text{Li}$ [16]. The constraint is roughly $\tilde{\tau}_{\tilde{\tau}} < 1000$ sec for $Y_{\tilde{\tau}} \gtrsim 10^{-15}$, while there is almost no constraint on stau lifetime for $Y_{\tilde{\tau}} \lesssim 10^{-15}$. It is also important for large $Y_{\tilde{\tau}}$ that the energetic hadrons produced by stau-decay modifies the abundance of D nuclei [17].

Stau abundance $Y_{\tilde{\tau}}$ depends on the value of the stau annihilation cross section, and hence on the stau annihilation process. In this paper, we consider the following three different parameter regions.

- (A) In most of the parameter region of the MSSM, the stau annihilation is dominated by the electroweak interaction.
- (B) When the $\tilde{\tau} - \tilde{\tau} - h$ coupling is large, the stau annihilation into the light CP-even Higgs bosons h is enhanced [7, 8].
- (C) When the $\tilde{\tau} - \tilde{\tau} - H$ coupling is large and the heavy Higgs mass satisfies the condition $m_H \simeq 2m_{\tilde{\tau}}$, the staus can annihilate at the resonance of the heavy Higgs boson H [8].

In the cases of (B) and (C), the stau abundance $Y_{\tilde{\tau}}$ can be significantly reduced compared to the case (A) [7, 8]. In the following subsections 2.2.1–2.2.3, we discuss the gravitino mass

upper bound for a given stau mass in these three different parameter regions. The obtained BBN bound on the gravitino mass is combined with the over-production bound discussed in Sec.2.1, which leads to the gluino mass upper bound for a given stau mass and reheating temperature.

2.2.1 (A) Stau Annihilation via Electroweak process

When the electroweak process is dominant, the stau abundance is estimated as [18]

$$Y_{\tilde{\tau}} \simeq 7 \times 10^{-14} \times \left(\frac{m_{\tilde{\tau}}}{100 \text{GeV}} \right). \quad (6)$$

Then, the bound from BBN on gravitino mass is [17]

$$m_{3/2} \lesssim \begin{cases} 0.4 \text{GeV} - 10 \text{GeV} & (100 \text{GeV} < m_{\tilde{\tau}} < 450 \text{GeV}) \\ 10 \text{GeV} - 20 \text{GeV} & (450 \text{GeV} < m_{\tilde{\tau}} < 1000 \text{GeV}) \end{cases}, \quad (7)$$

where the constraint in the region $100 \text{GeV} < m_{\tilde{\tau}} < 450 \text{GeV}$ comes from the bound on ${}^6\text{Li}$ overproduction by the catalyzed effect, whereas the bound on the hadronic decay of staus gives the constraint in the region $450 \text{GeV} < m_{\tilde{\tau}} < 1000 \text{GeV}$.

This upper bound on the gravitino mass can be easily translated into the upper bound on the gluino mass for a given stau mass and a reheating temperature. As we can see from Eq.(1) and Eq.(4), the upper bound on the gluino mass also depends on the other gaugino masses. In Fig.2, we show the upper bound on the gluino mass for a given gaugino masses and reheating temperature. We set the stau mass to be 300 GeV in the figure. We find the heavier gaugino masses lead to the more stringent upper bound on the gluino mass.

In the following discussion, we show the upper bounds on the gluino mass for the following two different gaugino mass relations:

- (i) $m_{\tilde{B}} = m_{\tilde{W}} = 1.1 m_{\tilde{\tau}}$. This gives almost the most conservative upper bound on the gluino mass (cf. Eq. (1)). Note that if $m_{\tilde{B}(\tilde{W})}$ is too degenerate with $m_{\tilde{\tau}}$, the stau abundance is enhanced by the $\tilde{B}(\tilde{W})$ decay, resulting in more stringent bounds on T_R (or $m_{\tilde{g}}$) [18].
- (ii) Gaugino masses satisfy the GUT relation, $m_{\tilde{B}}/g_1^2(m_{\tilde{B}}) = m_{\tilde{W}}/g_2^2(m_{\tilde{W}}) = m_{\tilde{g}}/g_3^2(m_{\tilde{g}})$, where $g_1(\mu)$, $g_2(\mu)$ and $g_3(\mu)$ are the running gauge coupling constants of $U(1)_Y$, $SU(2)_L$ and $SU(3)_C$ gauge symmetries at the mass scale μ respectively. This is the case for the minimal supergravity and the minimal gauge mediation models.

Fig. 3 and 4 show the results for the cases (i) and (ii), respectively. From the figures, we find the followings;

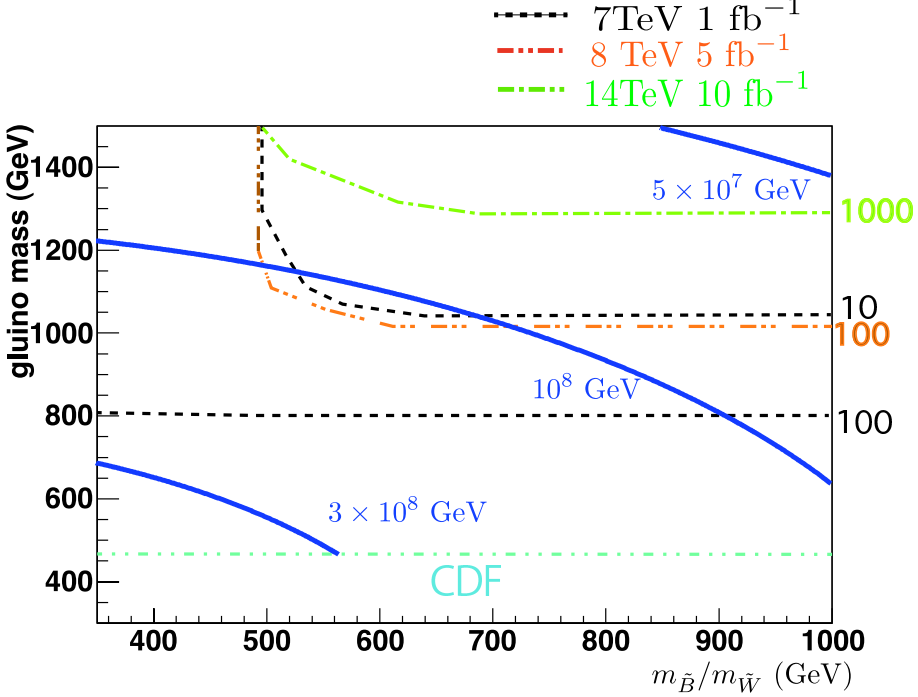


Figure 2: The upper bound on the gluino mass for the case (A), where the stau annihilation is dominated by the electroweak processes. The bino and wino masses are varied assuming $m_{\tilde{B}} = m_{\tilde{W}}$, while the stau mass is fixed as $m_{\tilde{\tau}} = 300\text{GeV}$. The solid (blue) lines are upper bounds on the gluino mass. We also plot the number of stau signatures at LHC with each \sqrt{s} and integrated luminosity. Here, the events only include the productions of gluinos, charginos and/or neutralinos (and staus), and we impose cuts and triggers. The horizontal dashed line around $m_{\tilde{g}} \simeq 470$ GeV comes from the CDF bound. We discuss the collider signature in Section 3.

- (i) $m_{\tilde{B}} = m_{\tilde{W}} = 1.1m_{\tilde{\tau}}$ case: the gluino mass cannot exceed about 2.4 TeV for $m_{\tilde{\tau}} < 1$ TeV and $T_R \gtrsim 10^8$ GeV. For $T_R > 3$ (5) $\times 10^8$ GeV, the stau mass is bounded as $m_{\tilde{\tau}} \lesssim 700$ (500) GeV, and the gluino mass is bounded as $m_{\tilde{g}} \lesssim 1100$ (700) GeV. There is no region for $T_R \gtrsim 7 \times 10^7$ GeV.
- (ii) The case of the GUT relation: the constraint on gluino mass and the reheating temperature are much severer than the case (i). There is no region for $T_R \gtrsim 7 \times 10^7$ GeV.

2.2.2 (B) Stau Annihilation with large stau-stau-light Higgs coupling

When the $\tilde{\tau} - \tilde{\tau} - h$ coupling is large, the stau annihilation into the light CP-even Higgs bosons h is enhanced [7, 8]. The trilinear coupling of the lighter stau and h is given by

$$\mathcal{L} = -\mathcal{A}_{\tilde{\tau} \tilde{\tau} h} \tilde{\tau}_1^* \tilde{\tau}_1 h, \quad (8)$$

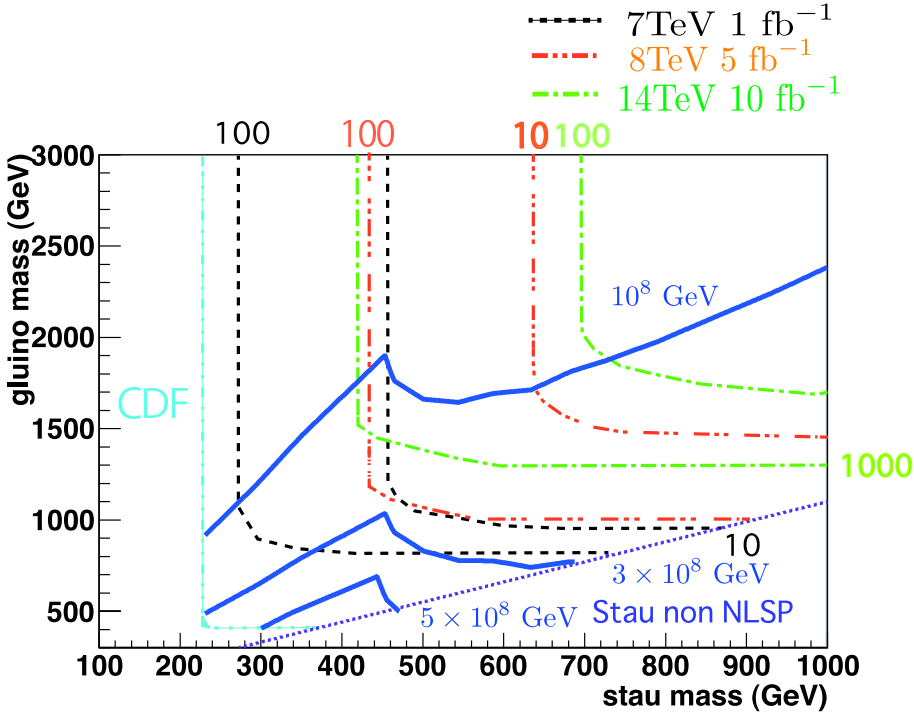


Figure 3: Case (A)-(i), where the stau annihilation is dominated by the electroweak interactions, and $m_{\tilde{B}} = m_{\tilde{W}} = 1.1 m_{\tilde{\tau}}$. The solid (blue) lines are upper bounds on the gluino mass for various reheating temperatures T_R . Contour plots of the number of expected SUSY events at LHC and the line of the CDF bound are shown in the same way as Fig. 2. The stau is not the LSP under the dotted (purple) line.

where the coefficient takes the form of

$$\begin{aligned} \mathcal{A}_{\tilde{\tau}\tilde{\tau}h^0} &\simeq -\frac{gm_{\tau}}{2M_W}(\mu\tan\beta + A_{\tau})\sin2\theta_{\tau} + \frac{gm_{\tau}^2}{M_W} \\ &\quad -g_Z M_Z \left[\left(-\frac{1}{2} + \sin^2\theta_W \right) \cos^2\theta_{\tau} - \sin^2\theta_W \sin^2\theta_{\tau} \right], \end{aligned} \quad (9)$$

where g , g_Z , M_W , M_Z , m_{τ} and θ_W are the Standard Model parameters, μ is the Higgsino mass parameter, $\tan\beta$ is the ratio of VEVs of the two Higgs doublets, and θ_{τ} is the mixing angle of the staus defined by

$$\begin{pmatrix} \tilde{\tau}_1 \\ \tilde{\tau}_2 \end{pmatrix} = \begin{pmatrix} \cos\theta_{\tau} & \sin\theta_{\tau} \\ -\sin\theta_{\tau} & \cos\theta_{\tau} \end{pmatrix} \begin{pmatrix} \tilde{\tau}_L \\ \tilde{\tau}_R \end{pmatrix}. \quad (10)$$

This trilinear coupling $\mathcal{A}_{\tilde{\tau}\tilde{\tau}h^0}$ is enhanced when μ , $\tan\beta$ and $\sin2\theta_{\tau}$ are large. The stau annihilation process via the large trilinear coupling may significantly reduce the stau abundance [7, 8].

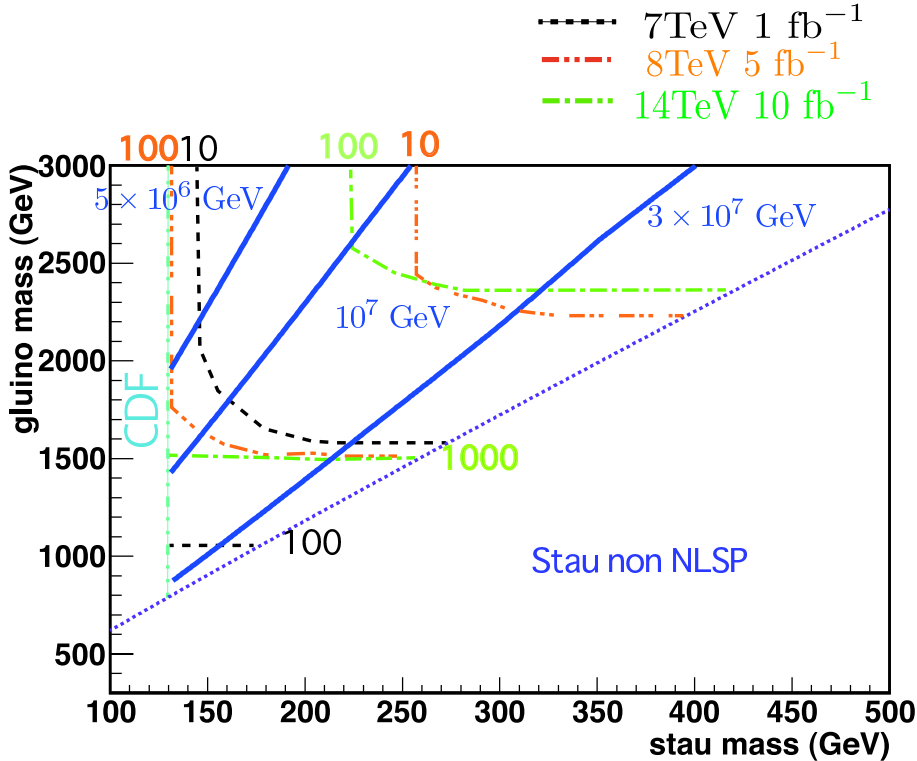


Figure 4: Case (A)-(ii), where the stau annihilation is dominated by the electroweak interactions, and the gaugino masses satisfy the GUT relation. The contour lines are the same as Fig. 3.

However, the large trilinear coupling may create disastrous charge/color breaking (CCB) minima in the $\tilde{\tau} - h$ potential [7]. In such a case, the vacuum in our universe is a local minimum, and therefore, our vacuum will eventually decay into a global minimum. The condition that the lifetime of our vacuum must be longer than the age of the universe, gives the upper bound on the value of $\mathcal{A}_{\tilde{\tau} h^0}$, as discussed in Appendix A. The resultant upper bound on $\mathcal{A}_{\tilde{\tau} h^0}$ is shown in Fig. 5 for $m_h = 120$ GeV.

The upper bound on $\mathcal{A}_{\tilde{\tau} h^0}$ gives the upper bound on the stau annihilation cross section. Since the relic abundance of the stau is given by

$$Y_{\tilde{\tau}} \simeq 1.0 \times 10^{-15} \left(\frac{10^{-5} \text{GeV}^{-2}}{\langle \sigma v \rangle} \right) \left(\frac{200 \text{GeV}}{m_{\tilde{\tau}}} \right), \quad (11)$$

the upper bound on the stau annihilation cross section gives the lower bound on $Y_{\tilde{\tau}}$, where σ is the annihilation cross section of stau, v is the relative velocity of staus and $\langle \rangle$ denotes the

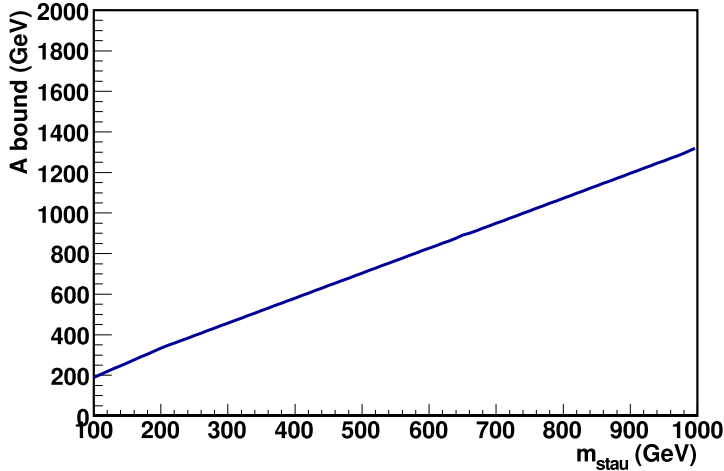


Figure 5: CCB bound on the stau-Higgs coupling $\mathcal{A}_{\tilde{\tau}\tilde{\tau}h^0}$ for $m_h = 120$ GeV. The constraint from the zero temperature decay rate is severer for $m_{\tilde{\tau}} > 220$ GeV, while the finite temperature transition dominates the bound for $m_{\tilde{\tau}} < 220$ GeV.

thermal average. In the large trilinear coupling case, $\langle \sigma v \rangle$ takes the form of

$$\langle \sigma v \rangle \simeq \frac{\mathcal{A}_{\tilde{\tau}\tilde{\tau}h^0}^4}{64\pi m_{\tilde{\tau}}^6} f_h + \frac{3Y_t^2 \mathcal{A}_{\tilde{\tau}\tilde{\tau}h^0}^2}{128\pi m_{\tilde{\tau}}^4} f_t, \quad (12)$$

where

$$f_h = \frac{\sqrt{1-r_h}}{(1-r_h/4)^2} \theta(1-r_h), \quad f_t = \frac{(1-r_t/2)\sqrt{1-r_t}}{(1-r_t/4)^2} \theta(1-r_t), \quad (13)$$

with $r_h = m_h^2/m_{\tilde{\tau}}^2$ and $r_t = m_t^2/m_{\tilde{\tau}}^2$. If $m_{\tilde{\tau}}$ is larger than m_h , the annihilation into Higgs bosons via the large trilinear coupling is possible, and the first term in Eq.(12) becomes nonzero. In the same way, the second term in Eq.(12) becomes nonzero when $m_{\tilde{\tau}}$ is larger than m_t . In the following, we take $m_h = 120$ GeV and $m_t = 173$ GeV. The lower bound on $Y_{\tilde{\tau}}$ in this large $\mathcal{A}_{\tilde{\tau}\tilde{\tau}h^0}$ scenario is shown in Fig.6. For comparison, we also show the $Y_{\tilde{\tau}}$ when the electroweak process is the dominant stau annihilation process in the same figure. We find that $Y_{\tilde{\tau}}$ in the large $\mathcal{A}_{\tilde{\tau}\tilde{\tau}h^0}$ scenario is significantly smaller than that of the electroweak annihilation, but it cannot be smaller than 10^{-15} . Therefore, the bound from the ${}^6\text{Li}$ overproduction by the catalyzed effect severely constrains the gravitino mass [17],

$$m_{3/2} \lesssim 0.4\text{GeV} - 115\text{GeV} \quad (100\text{GeV} < m_{\tilde{\tau}} < 1000\text{GeV}) \quad (14)$$

as shown in Fig.7.

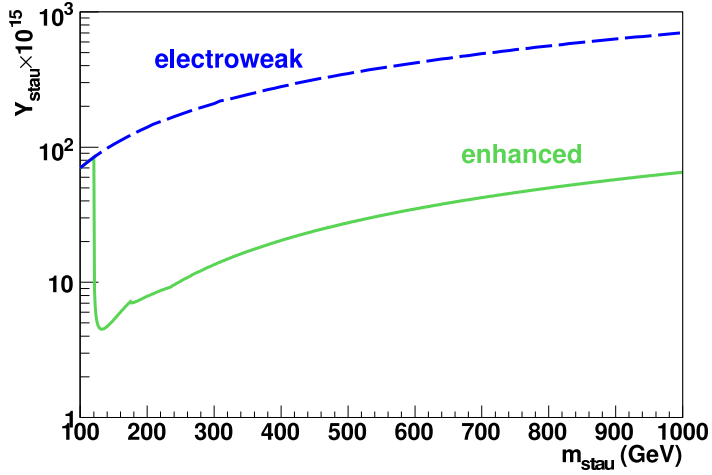


Figure 6: Green solid line: $Y_{\tilde{\tau}}$ vs $m_{\tilde{\tau}}$ when $A_{\tilde{\tau}\tilde{\tau}h}$ is the maximal value. We take $m_h = 120$ GeV and $m_t = 173$ GeV. Blue dashed line: $Y_{\tilde{\tau}}$ when the electroweak process is the dominant stau annihilation process.

This gravitino mass upper bound leads to the upper bound on the gluino mass for a given stau mass and reheating temperature. As in the case in Section 2.2.1, we show the upper bounds on the gluino mass with the two gaugino mass relations: (i) $m_{\tilde{B}} = m_{\tilde{W}} = 1.1m_{\tilde{\tau}}$, and (ii) the GUT relation. The upper bound with the relation (i) is shown in Fig.8, while that with the relation (ii) is shown in Fig.9. From Fig.8 and Fig.9, we find the followings;

- (i) $m_{\tilde{B}} = m_{\tilde{W}} = 1.1m_{\tilde{\tau}}$ case: the behavior of the gluino mass upper bound in Fig.8 are similar to that in Fig.3 for $m_{\tilde{\tau}} \leq 450$ GeV, since the gravitino mass upper bound is determined by the constraints from ${}^6\text{Li}$ in the region. On the other hand, the behavior is quite different for $m_{\tilde{\tau}} > 450$ GeV, because the gravitino mass upper bound in the case (A) is determined by the constraints from the deuterium, while the upper bound in the case (B) is still determined by the constraints from ${}^6\text{Li}$. It is also remarkable that $T_R > 10^9$ GeV is possible.
- (ii) The case of the GUT relation: the behavior of the gluino mass upper bound is almost the same as Fig.4. We also see that the behavior of the gluino mass bound slightly changes at $m_{\tilde{\tau}} = m_t$, because the annihilation into top quark becomes possible for $m_{\tilde{\tau}} > m_t$.

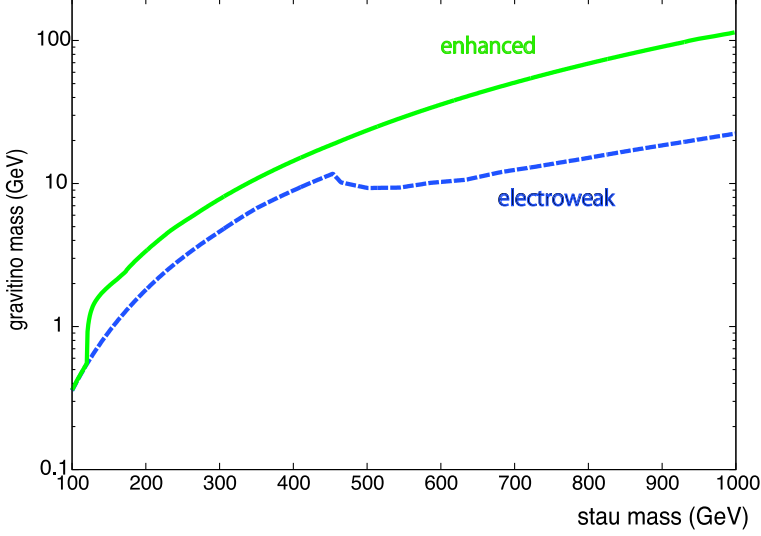


Figure 7: Green solid line: gravitino mass bound for the case with an enhanced h -stau coupling. Blue dashed line: gravitino mass bound for the case of the electroweak annihilation.

2.2.3 (C) Stau Annihilation near the pole of the Heavy Higgs Boson

The stau annihilation cross section can be considerably enhanced in case that $m_H \simeq 2m_{\tilde{\tau}}$ and A_τ , $\tan\beta$ and $\sin 2\theta_\tau$ are large [8]. The trilinear coupling of the lightest stau with H takes the form of

$$\mathcal{L} = -\mathcal{A}_{\tilde{\tau}\tilde{\tau}H} \tilde{\tau}_1^* \tilde{\tau}_1 H, \quad (15)$$

where the coefficient is given by

$$\mathcal{A}_{\tilde{\tau}\tilde{\tau}H} \simeq -\frac{gm_\tau}{2M_W} (A_\tau \tan\beta - \mu) \sin 2\theta_\tau + \frac{gm_\tau^2}{M_W} \tan\beta. \quad (16)$$

in the large $\tan\beta$ region. When $A_\tau \tan\beta$ is large, the first term in the right hand side becomes enhanced. In such large $A_\tau \tan\beta$ case, the annihilation through H exchange can be the dominant process, and if m_H satisfies the resonance condition $m_H \simeq 2m_{\tilde{\tau}}$, it is enhanced greatly.

The large $\mathcal{A}_{\tilde{\tau}\tilde{\tau}H}$ may generate the disastrous CCB minimum, and therefore, the value of $\mathcal{A}_{\tilde{\tau}\tilde{\tau}H}$ is constrained as in the case of the enhanced h -stau trilinear coupling. We obtain the upper bound on $\mathcal{A}_{\tilde{\tau}\tilde{\tau}H}$ as we discuss in Appendix A. The bound on $\mathcal{A}_{\tilde{\tau}\tilde{\tau}H}$ is shown in Fig. 10 for $m_H = 2m_{\tilde{\tau}}$.

In this case, the stau relic abundance can be sufficiently reduced to avoid the BBN constraint, i.e., $Y_{\tilde{\tau}} < 10^{-15}$. For illustration, we take $m_H = 2m_{\tilde{\tau}}$ and $\mathcal{A}_{\tilde{\tau}\tilde{\tau}H} = 1.3 \times m_{\tilde{\tau}}$, which

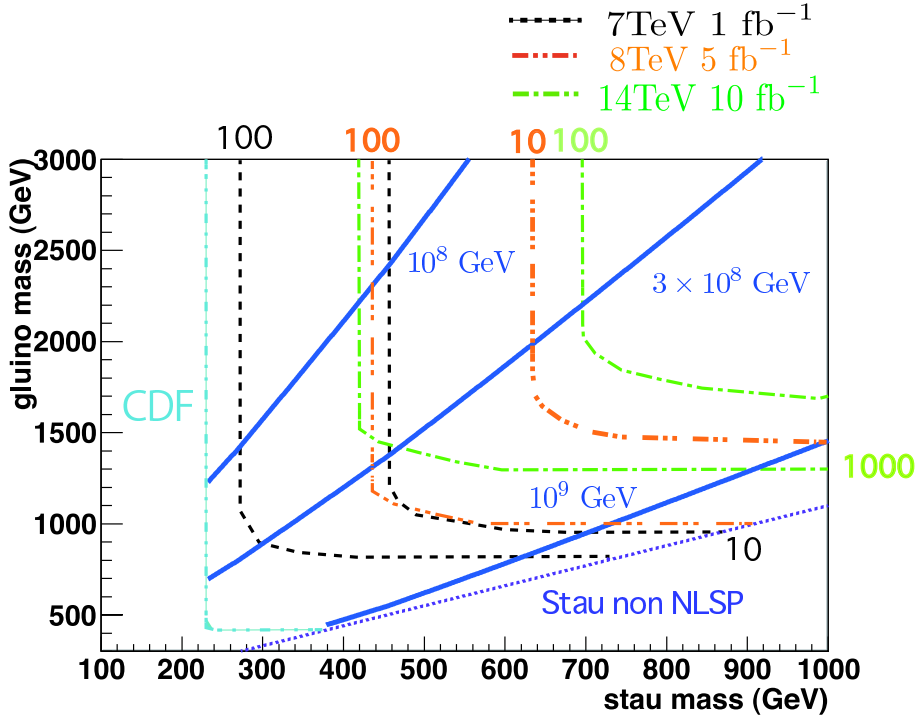


Figure 8: Case (B)-(i), where the stau annihilation is enhanced by the h -stau-coupling, and $m_{\tilde{B}} = m_{\tilde{W}} = 1.1 m_{\tilde{\tau}}$. The contour lines are the same as Fig. 3.

is below the upper bound on $\mathcal{A}_{\tilde{\tau}\tilde{\tau}H}$ in $100\text{GeV} < m_{\tilde{\tau}} < 1000\text{GeV}$, as can be seen from Fig. 10. The resultant abundance $Y_{\tilde{\tau}}$ is shown in Fig. 11, where we use the program `micrOMEGA2.4` [22] to calculate the relic abundance. We see that $Y_{\tilde{\tau}}$ can be less than 10^{-15} for $100\text{GeV} < m_{\tilde{\tau}} < 1000\text{GeV}$, and therefore BBN does not provide any constraints on the gravitino mass.

There is another constraint from the CMB spectrum distortion [23]. However, the difference between the stau mass and the gravitino mass upper bound $m_{3/2}^{\max}$ is small, $(m_{\tilde{\tau}} - m_{3/2}^{\max}(m_{\tilde{\tau}}))/m_{\tilde{\tau}} \lesssim 0.01$. Thus, we take $m_{3/2}^{\max}(m_{\tilde{\tau}}) = m_{\tilde{\tau}}$, for simplicity.

The upper bound on the gravitino mass leads to the upper bound on the gluino mass for a given stau mass and reheating temperature. As in the case in Section 2.2.1 and Section 2.2.2, we show the gluino mass upper bound (i) for $m_{\tilde{B}} = m_{\tilde{W}} = 1.1 \times m_{\tilde{\tau}}$ in Fig. 12, and (ii) when there is the GUT relation between gaugino masses in Fig. 13. Note that, in the larger stau mass region, the gluino mass is maximized when the gravitino mass is smaller than $m_{3/2}^{\max}(m_{\tilde{\tau}})$. That is because the upper bound on the gluino mass drops down in the higher gravitino mass region as shown in Fig. 1. From Fig. 12 and Fig. 13, we find followings;

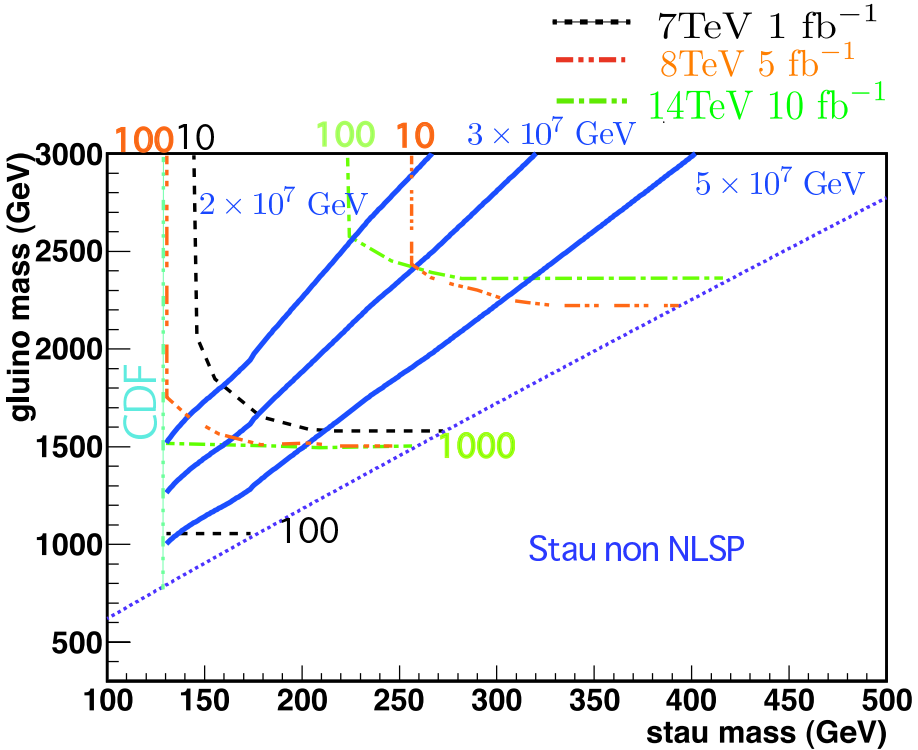


Figure 9: Case (B)-(ii), where the stau annihilation is enhanced by the h -stau-coupling, and the gaugino masses satisfy the GUT relation. The contour lines are the same as Fig. 3.

- (i) $m_{\tilde{B}} = m_{\tilde{W}} = 1.1 \times m_{\tilde{\tau}}$ case: Interestingly, $T_R > 2 \times 10^9$ GeV which is required by thermal leptogenesis is possible in the region $m_{\tilde{\tau}} \lesssim 1500$ GeV. We can even achieve $T_R > 5 \times 10^9$ GeV. The gluino mass bound becomes lower in the larger $m_{\tilde{\tau}}$ region because the Bino mass and the Wino mass becomes heavier for large stau mass, and the constraints of the gravitino overclosure becomes severer.
- (ii) When there is the GUT relation: $T_R > 2 \times 10^9$ GeV is possible in $m_{\tilde{\tau}} \lesssim 350$ GeV. The gluino mass is bounded as $m_{\tilde{g}} \lesssim 2$ TeV when $T_R > 2 \times 10^9$ GeV.

3 Collider Signatures

Let us study the collider detectability of the scenario of the high reheating temperature. In the previous section, it was shown that the gluino mass is constrained to be less than a few TeV to realize a high reheating temperature. Light SUSY particles have been already excluded by direct searches in Tevatron, while TeV colored SUSY particles are in the reach of sensitivity of LHC. If heavy SUSY particles are produced at a collision, they subsequently decays into

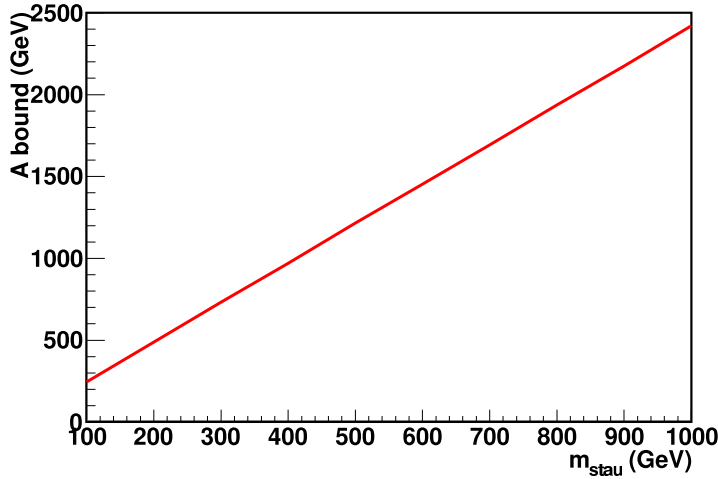


Figure 10: CCB bound on the stau-Higgs coupling $\mathcal{A}_{\tilde{\tau}\tilde{\tau}H}$. The finite temperature transition dominates the bound for $m_{\tilde{\tau}} > 100$ GeV.

lighter SUSY particles with radiating SM particles, and promptly generate the NLSP stau in the end of the decay chain. Since the gravitino mass is as large as $\mathcal{O}(1 - 100)$ GeV in the high reheating temperature scenario, the NLSP stau is long-lived enough to be observed as a stable particle in the detectors. Noting that the stau has an electromagnetic charge, we expect the events with charged tracks when SUSY particles are produced at collisions. In this section, we discuss the Tevatron bound and the LHC sensitivity of the high reheating temperature scenario.

Before proceeding to the collider study, we summarize the tools for the numerical analysis. We use PYTHIA 6.4.22 [24] to study the kinematics and to estimate the cross sections except for those of the colored SUSY particle productions. The gluino and squark production cross sections are estimated by the program Prospino2 [25] at the NLO level. The Tevatron and LHC detectors are simulated by the package PGS4 [26].

3.1 Tevatron Bound

At the Tevatron experiments, the stau is expected to behave as a heavy muon, namely a charged massive and long-lived particle. As long as the stau has a large velocity, it is not distinguishable from the muon. When the transverse momentum, p_T , of the muon is large, it has a large velocity of $\beta \simeq 1$, while the stau is likely to have a lower speed. Such a high- p_T and low speed “muon” has been searched for in Tevatron by measuring the time of flight

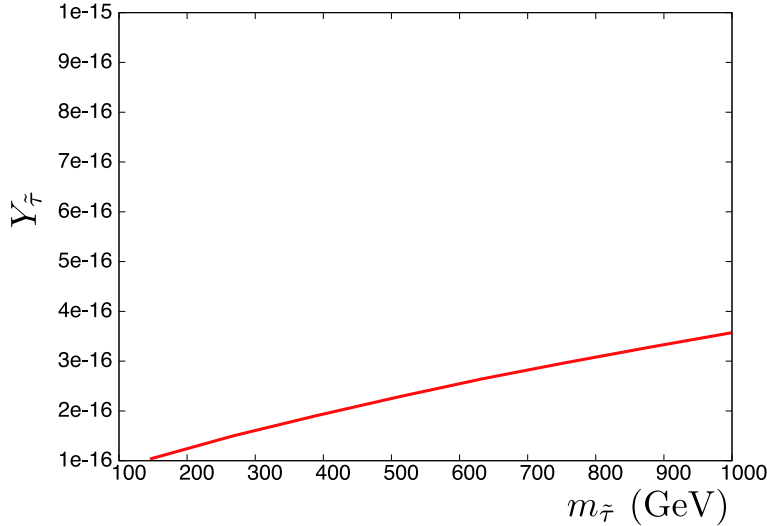


Figure 11: $Y_{\tilde{\tau}}$ vs $m_{\tilde{\tau}}$ when $\mathcal{A}_{\tilde{\tau}\tilde{\tau}H} = 1.3 \times m_{\tilde{\tau}}$, and $m_H = 2m_{\tilde{\tau}}$.

[27, 28]. According to [27], the events are selected by the following trigger:

- the highest p_T “muon” candidate has p_T larger than 20 GeV which satisfies an isolation condition $E_T(0.4)/p_T(\mu) < 0.1$,

where $E_T(0.4)$ is the sum of the transverse energy within a cone $R = 0.4$ around the candidate, excluding the energy deposited by the muon candidate itself, and $p_T(\mu)$ is the transverse momentum of the highest p_T muon candidate. Note that the long-lived charged massive particle is identified as a “muon” candidate. The events that satisfy the above trigger condition are read out. The Tevatron constraint is that the production cross section of the long-lived charged massive particle which runs toward the direction $|\eta| < 0.7$ with $p_T > 40$ GeV, and with the velocity $0.4 < \beta < 0.9$, is smaller than 10 fb at the 95% C.L.. The constraint gives the lower bound on masses of SUSY particles.

We show the constraints from Tevatron in Figs.2–4, Fig.8, Fig.9, Fig.12 and Fig.13. The constraints in Fig.3, Fig.8, and Fig.12 are the same, which corresponding to the cases (A)-(i), (B)-(i), and (C)-(i), respectively. Similarly, the constraints in Fig.4, Fig.9, and Fig.13 (corresponding to the cases (A)-(ii), (B)-(ii), and (C)-(ii), respectively) are the same. We only consider productions of the gauginos and the lighter staus, and do not consider the production of the other scalar particles. This is realized when their masses are relatively heavy. In the case that the gluino mass is relatively small, gluino pair production is the main production channel. That is the case in the regions around the horizontal lines in Fig.2, Fig.3, Fig.8 and

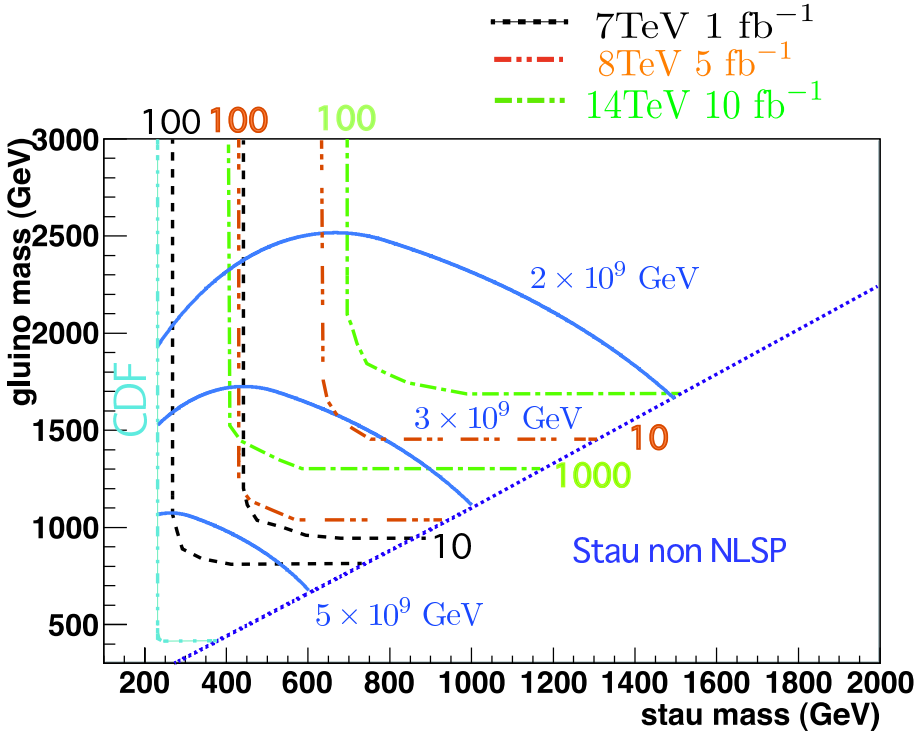


Figure 12: Case (C)-(i), where $m_H \simeq 2m_{\tilde{\tau}}$ and the H -stau-coupling is enhanced, and $m_{\tilde{B}} = m_{\tilde{W}} = 1.1 m_{\tilde{\tau}}$. The contour lines are the same as Fig. 3.

Fig.12. When the gluino mass is large, the stau direct production, chargino-neutralino and chargino-chargino pair productions are the main production channel. The vertical lines of the CDF constraints in Fig.3 are determined by the chargino-neutralino and chargino-chargino pair production cross sections. The same situation holds in the regions around the vertical lines in Fig.8 and Fig.12. On the other hand, the vertical line in Fig.4 is determined by the stau direct production. That is also the case in the regions around the vertical lines in Fig.9 and Fig.13.

3.2 LHC signatures

The scenarios of the high reheating temperature predict the gluino mass being less than a few TeV. Although the Tevatron energy is not large enough to cover the mass range, the LHC is suited for detecting the particle. The LHC is running at the center-of-mass energy $\sqrt{s} = 7$ TeV and the integrated luminosity is planned to become up to a few fb^{-1} in 2011. The schedule of 2012 is still in discussion: an optimistic scenario is $\sqrt{s} = 8$ TeV with $L_i \sim 10 \text{ fb}^{-1}$. After the upgrade, the collider is aimed to run at $\sqrt{s} = 14$ TeV. In the following, we

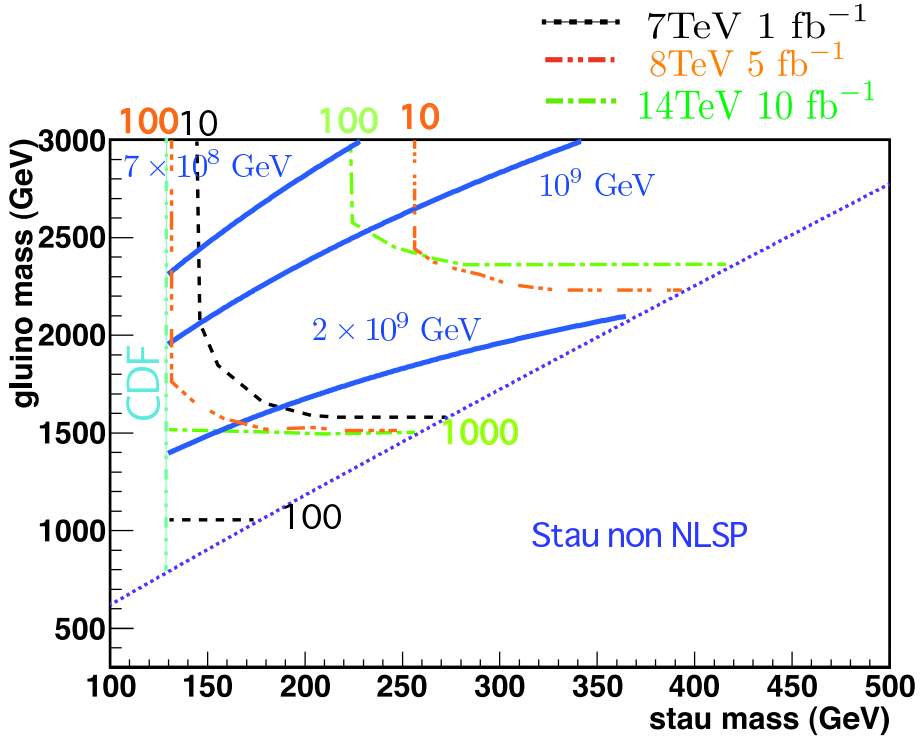


Figure 13: Case (C)-(ii), where $m_H \simeq 2m_{\tilde{\tau}}$ and the H -stau-coupling is enhanced, and the gaugino masses satisfy the GUT relation. The contour lines are the same as Fig. 3.

discuss the LHC sensitivity of the high reheating temperature scenario in the three setups: $\sqrt{s} = 7$ TeV with $L_i = 1 \text{ fb}^{-1}$, $\sqrt{s} = 8$ TeV with $L_i = 5 \text{ fb}^{-1}$ and $\sqrt{s} = 14$ TeV with $L_i = 10 \text{ fb}^{-1}$.

Analogous to the Tevatron, the stau signature is the charged track of the low speed muon-like particle with high p_T within the detectors. First of all, the SUSY events are selected by imposing a trigger menu, and then analyzed off-line with cut conditions in order to be distinguished from the background. In the following analysis, we impose the following trigger conditions,

- at least one isolated electron has $p_T > 20 \text{ GeV}$,
- at least one isolated muon has $p_T > 40 \text{ GeV}$,
- at least one isolated tau has $p_T > 100 \text{ GeV}$,
- at least one jet has $p_T > 200 \text{ GeV}$,
- at least three jet has $p_T > 100 \text{ GeV}$,
- at least one isolated stau has $p_T > 40 \text{ GeV}$ within the bunch,

- at least two staus have $p_T > 40$ GeV within the bunch.

If any one of these conditions is satisfied, the event is read out. In our simulation, the isolation conditions on the electron and the tau relies on PGS4, while those of the muon and the stau are

1. the summed p_T in a $R = 0.4$ cone around the particle (excluding the particle itself) is less than 5 GeV,
2. the ratio of E_T in a 3×3 calorimeter array around the particle (including the particle's cell) to p_T of the particle is less than 0.1125.

The bunch condition, i.e., the condition that the stau has a velocity large enough to reach the muon trigger detector before the next bunch collides, is necessary for the stau triggers, since otherwise they do not work correctly [30]. We require $\beta > 0.7$ for the stau propagating in the barrel region ($|\eta| < 1.0$) and $\beta > 0.8$ in the endcap region ($1.0 < |\eta| < 2.8$) [29].

Among the events that are read out by the triggers, the SUSY signals are required to satisfy the following cut conditions,

- $p_T > 20$ GeV
- $0.5 < \beta < 0.9$
- $|\eta| < 2.5$.

Although the muon productions are the relevant standard model backgrounds of the stau signals, they are significantly reduced to be almost zero by especially the first two cuts, since the high p_T muons have $\beta \simeq 1$. The last condition is added because the stau is detected in the muon detector [29, 30].

The number of events is reduced to roughly 50% \sim 90% by the above trigger conditions. When the stau direct production or chargino/neutralino pair production is the dominant production channel, roughly a half of the triggered events are selected by the stau and the others are selected by jets and taus. On the other hand, when the gluino production is dominant, most of the triggered events are selected by jets and taus. Note that we put the trigger efficiency as unity for simplicity. In the real detector system, however, the efficiency for single jet and for single tau is not good. Thus the number of the events selected only by single jet or single tau (roughly 10% \sim 40% of the triggered events) may be further reduced if we consider the trigger efficiency.

We also have to consider the reconstruction efficiency of the stau. The reconstruction

efficiency varies from 0.1 to 0.9 for $\beta \simeq 0.5 \sim 0.9$ according to ATLAS CSC studies [29]. The analysis can be improved by the method studied in [30], which provides the efficiency more than 90% for $\beta \gtrsim 0.5$. In the following, we assume the efficiency for the stau with $\beta > 0.5$ to be 100% and for the stau with $\beta \leq 0.5$ to be zero for simplicity.

In Fig.2–4, Fig.8, Fig.9, Fig.12 and Fig.13, we show the number of stau signals that satisfy the trigger conditions and the cut conditions at LHC for $\sqrt{s} = 7$ TeV with $L_i = 1 \text{ fb}^{-1}$, $\sqrt{s} = 8$ TeV with $L_i = 5 \text{ fb}^{-1}$, and $\sqrt{s} = 14$ TeV with $L_i = 10 \text{ fb}^{-1}$. The contour lines in Fig.3, Fig.8, and Fig.12 are the same, which corresponding to the cases (A)-(i), (B)-(i), and (C)-(i), respectively. Likewise, the contour lines in Fig.4, Fig.9, and Fig.13 (corresponding to the cases (A)-(ii), (B)-(ii), and (C)-(ii), respectively) are identical. We only consider gaugino production and stau direct production at the collision as the production channels, and do not consider the production of the other scalar particles. As in the case of the Tevatron constraints, the gluino pair production is the main channel if the gluino mass is relatively small. That is the case in the regions around the horizontal lines in Fig.2, Fig.3, Fig.8 and Fig.12. When the gluino mass is large, the stau direct production, chargino-neutralino and chargino-chargino pair productions are the main production channel. The vertical lines of the LHC signatures in Fig.2 are determined by the chargino-neutralino and chargino-chargino pair production cross sections. The same situation holds in the regions around the vertical lines in Fig.3, Fig.8, Fig.12, and the horizontal lines in Fig.4, Fig.9, Fig.13. On the other hand, the vertical line in Fig.4 is determined by the stau direct production. That is also the case in the regions around the vertical lines in Fig.9 and Fig.13.

Now let us discuss the implications of these LHC signatures on the reheating temperature. Combining the cosmological upper bound on the gluino mass discussed in Sec. 2 with the results obtained in this section, we can see the minimal number of stau signals in each reheating temperature. For example, if T_R is larger than 3×10^8 GeV and the main stau annihilation process is the electroweak process, more than 10 staus are observed for $\sqrt{s} = 7$ TeV with $L_i = 1 \text{ fb}^{-1}$. Also, more than 10 staus are observed for $\sqrt{s} = 14$ TeV and $L_i = 10 \text{ fb}^{-1}$, if T_R is larger than 10^8 GeV, $m_{\tilde{\tau}} < 1000$ GeV, and the electroweak process is dominant. In TABLE 1, we summarize the range of the reheating temperature with which more than 10 stau signals are expected in each scenario, \sqrt{s} , and L_i . It is remarkable that $T_R \gtrsim 2 \times 10^9$ GeV which is required by the thermal leptogenesis is all covered at $\sqrt{s} = 14$ TeV and $L_i = 10 \text{ fb}^{-1}$.

Although we have considered only gaugino production and stau direct production at the collisions when discussing the Tevatron constraint and LHC signatures, gluino-squark

Annihilation Process	Gaugino Masses	\sqrt{s}, L_i	Covered reheating temperature
(A) electroweak	(i) $m_{\tilde{B}} = m_{\tilde{W}} = 1.1m_{\tilde{\tau}}$ (Fig. 3)	7TeV, 1fb^{-1}	$T_R \gtrsim 3 \times 10^8 \text{ GeV}$
		8TeV, 5fb^{-1}	$T_R \gtrsim 10^8 \text{ GeV}$ for $m_{\tilde{\tau}} \lesssim 600 \text{ GeV}$
		14TeV, 10fb^{-1}	$T_R \gtrsim 10^8 \text{ GeV}$ for $m_{\tilde{\tau}} \lesssim 1000 \text{ GeV}$
	(ii) GUT relation (Fig. 4)	7TeV, 1fb^{-1}	$T_R \gtrsim 3 \times 10^7 \text{ GeV}$ for $m_{\tilde{\tau}} \lesssim 200 \text{ GeV}$
		8TeV, 5fb^{-1}	$T_R \gtrsim 3 \times 10^7 \text{ GeV}$ for $m_{\tilde{\tau}} \lesssim 300 \text{ GeV}$
		14TeV, 10fb^{-1}	$T_R \gtrsim 3 \times 10^7 \text{ GeV}$ for $m_{\tilde{\tau}} \lesssim 400 \text{ GeV}$
(B) enhanced by large $\mathcal{A}_{\tilde{\tau}\tilde{\tau}h}$	(i) $m_{\tilde{B}} = m_{\tilde{W}} = 1.1m_{\tilde{\tau}}$ (Fig. 8)	7TeV, 1fb^{-1}	$T_R \gtrsim 10^9 \text{ GeV}$ for $m_{\tilde{\tau}} \lesssim 700 \text{ GeV}$
		8TeV, 5fb^{-1}	$T_R \gtrsim 10^9 \text{ GeV}$ for $m_{\tilde{\tau}} \lesssim 1000 \text{ GeV}$
		14TeV, 10fb^{-1}	$T_R \gtrsim 3 \times 10^8 \text{ GeV}$ for $m_{\tilde{\tau}} \lesssim 900 \text{ GeV}$
	(ii) GUT relation (Fig. 9)	7TeV, 1fb^{-1}	$T_R \gtrsim 5 \times 10^7 \text{ GeV}$ for $m_{\tilde{\tau}} \lesssim 200 \text{ GeV}$
		8TeV, 5fb^{-1}	$T_R \gtrsim 5 \times 10^7 \text{ GeV}$ for $m_{\tilde{\tau}} \lesssim 300 \text{ GeV}$
		14TeV, 10fb^{-1}	$T_R \gtrsim 5 \times 10^7 \text{ GeV}$ for $m_{\tilde{\tau}} \lesssim 400 \text{ GeV}$
(C) enhanced by large $\mathcal{A}_{\tilde{\tau}\tilde{\tau}H}$ near the pole of H	(i) $m_{\tilde{B}} = m_{\tilde{W}} = 1.1m_{\tilde{\tau}}$ (Fig. 12)	7TeV, 1fb^{-1}	$T_R \gtrsim 5 \times 10^9 \text{ GeV}$
		8TeV, 5fb^{-1}	$T_R \gtrsim 3 \times 10^9 \text{ GeV}$
		14TeV, 10fb^{-1}	$T_R \gtrsim 2 \times 10^9 \text{ GeV}$
	(ii) GUT relation (Fig. 13)	7TeV, 1fb^{-1}	$T_R \gtrsim 2 \times 10^9 \text{ GeV}$ for $m_{\tilde{\tau}} \lesssim 200 \text{ GeV}$
		8TeV, 5fb^{-1}	$T_R \gtrsim 10^9 \text{ GeV}$ for $m_{\tilde{\tau}} \lesssim 250 \text{ GeV}$
		14TeV, 10fb^{-1}	$T_R \gtrsim 2 \times 10^9 \text{ GeV}$

Table 1: The range of the reheating temperature with which more than 10 stau signals are expected in each scenario.

production becomes dominant when the squark mass is relatively light. We show the Tevatron constraint and LHC signatures in Fig.14 when the squark mass $m_{\tilde{q}}$ equals to $m_{\tilde{g}}$ and the gaugino masses satisfy the condition (i), $m_{\tilde{B}} = m_{\tilde{W}} = 1.1m_{\tilde{\tau}}$. We also show the upper bound on the gluino mass in the case of (A)-(i). The cross section of gluino-squark pair production is roughly ten times larger than the gluino pair production. Thus, in the region where the gluino pair production is dominant in Fig.3, the expected number of stau signals increase in this light squark case. As can be seen from Fig. 14, the contour lines of the constant stau number shift upwards by $\Delta m_{\tilde{g}} \simeq 200 \sim 400 \text{ GeV}$, compared with Fig. 3. On the other hand, the result does not change very much when there is the GUT relation even for $m_{\tilde{q}} \simeq m_{\tilde{g}}$. That is because the gluino production is not the dominant channel of the SUSY events in the regions around the vertical lines and the horizontal lines of, e.g., Fig.4.

4 Conclusion and Discussion

In this paper, the observability of the stau signals at LHC has been studied in the scenario with the gravitino LSP and the stau NLSP under the cosmological constraints. It was seen that a

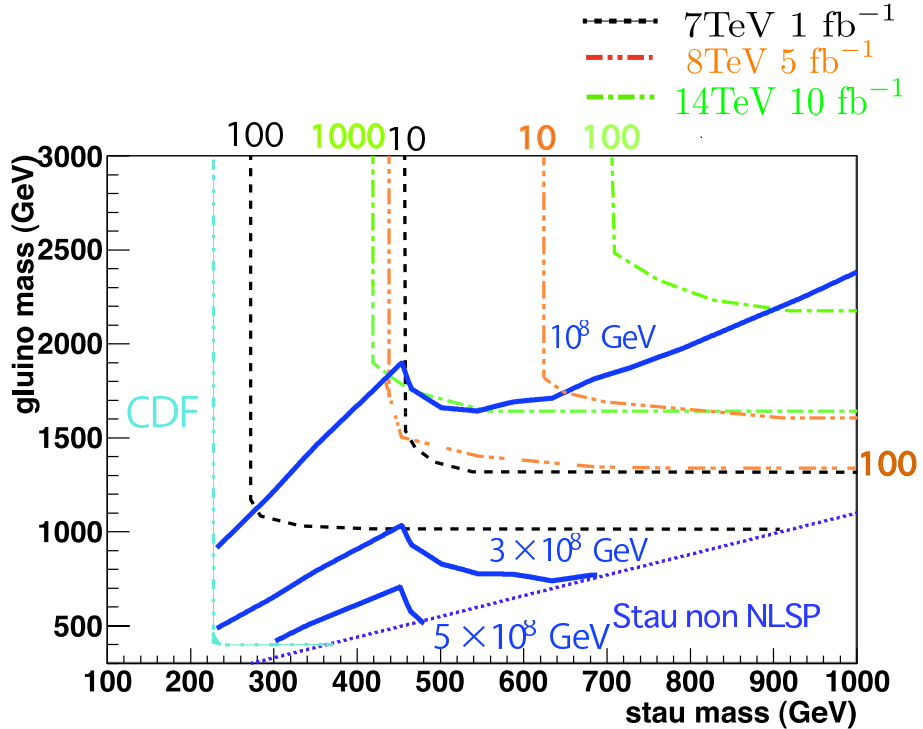


Figure 14: Same as Fig.3 but with $m_{\text{squark}} \simeq M_3$.

higher reheating temperature predicts a lower gluino mass, and therefore more stau signals can be observed at LHC. The upper bound on the gluino mass depends on the annihilation process of the stau, and we have considered three cases that (A) the annihilation is dominated by the electroweak processes, (B) the stau annihilation into the light Higgs boson is enhanced, and (C) the stau annihilation takes place near the pole of the heavy Higgs. In the case (A), which is true in most of the MSSM parameter region, the reheating temperature cannot be larger than 7×10^8 GeV. If we further assume that the gaugino masses satisfy the GUT relation, the upper bound becomes severer and it cannot exceed 7×10^7 GeV. On the other hand, the reheating temperature can be much higher for the cases (B) and (C). Especially, we saw that the reheating temperature can be as large as $T_R > 2 \times 10^9$ GeV, which is required by the thermal leptogenesis, in the case (C) even if the gaugino masses satisfy the GUT relation.

We have then investigated the Tevatron constraints and the LHC signatures of the long-lived staus by imposing the trigger and the cut conditions. We found that, when the stau annihilates mainly via the electroweak process, it is expected that more than 10 stau signals are observed at the first stage of LHC with $\sqrt{s} = 7\text{TeV}$ and $L_i = 1\text{fb}^{-1}$ in the region where T_R is larger than 3×10^8 GeV. When the heavy Higgs boson effectively contributes

to the stau annihilation, the first stage of LHC has a sensitivity to the parameter region of $T_R > 5 \times 10^9$ GeV. The LHC sensitivity improves greatly as the collider energy and the luminosity increase. The stau signals will be detected if T_R exceeds 10^8 GeV as long as $m_{\tilde{\tau}} \lesssim 1000$ GeV. It is also emphasized that all the regions which satisfy $T_R > 2 \times 10^9$ GeV can be checked by LHC with $\sqrt{s} = 14$ TeV and $L_i = 10\text{fb}^{-1}$.

We have also studied a specific case of the gaugino mass spectrum, i.e. the GUT relation. The LHC sensitivity as well as the cosmological constraint on the gluino mass is sensitive to the gaugino mass spectrum. The cosmological upper bound becomes severer than the case with generic gaugino masses, while at LHC the chargino and/or neutralino channels dominate the productions of the SUSY events instead of the channels of the colored (gluino) SUSY particles, especially for a low gluino mass region. It was found that the LHC has a detection sensitivity for lower reheating temperature models.

In this paper, we have assumed that there is no entropy production after the reheating epoch. However, our results can also be applied to the case with an entropy production, by replacing the reheating temperature T_R with $T_R^{\text{eff}} = T_R/\Delta$, where Δ is the dilution factor of the gravitino abundance. Even if the entropy production occurs after the freeze-out of the stau and before the BBN, the results of the case (C) (Figs.12 and 13), where there is no BBN constraint, hold for T_R^{eff} .

It is usually difficult to probe the reheating epoch of the universe directly. Nonetheless, the LHC has a sensitivity to the high reheating temperature models, as we discussed in this paper. Once heavy charged tracks will be observed at LHC, the reheating temperature receives an upper bound, depending on the SUSY mass spectrum. This enables us to reveal features of the early universe.

Acknowledgment

The work of K.H. was supported by JSPS Grant-in-Aid for Young Scientists (B) (21740164) and Grant-in-Aid for Scientific Research (A) (22244021). The work of K.N. was supported by JSPS Grant-in-Aid for JSPS Fellows. This work was supported by World Premier International Center Initiative (WPI Program), MEXT, Japan.

A Vacuum stability constraint on the stau trilinear coupling

In this appendix, the vacuum constraint on the stau trilinear coupling is discussed, which is used in Sec. 2.2.2 and Sec. 2.2.3. The lifetime of our vacuum can be estimated by using the ‘‘bounce method’’ [20]. By using the euclidian action $S_E[\bar{\phi}]$ with the bounce solution $\bar{\phi}$, the decay rate of the false vacuum per unit volume is estimated by

$$\Gamma/V \simeq E^4 \exp \left[-S_E[\bar{\phi}] \right], \quad (17)$$

where E is the typical energy scale of the potential. We put the value of the potential energy at the global minimum of the potential as 0. Since the lifetime of our vacuum must be longer than the age of the universe,

$$\Gamma/V \times \left(\frac{1}{H_0} \right)^4 \ll 1 \quad (18)$$

must be satisfied, where H_0 is present Hubble constant. This constraint gives the lower bound on the bounce,

$$S_E[\bar{\phi}] \gtrsim 400. \quad (19)$$

Let us start from the case that the $\tilde{\tau}$ - $\tilde{\tau}$ - h trilinear coupling $\mathcal{A}_{\tilde{\tau}\tilde{\tau}h^0}$ is large. In our analysis, the euclidian action takes the form of

$$S_E[\tilde{\tau}, h] = \int_{-\infty}^{\infty} d^4 x_E \left[\frac{1}{2} (\partial_i \tilde{\tau}) (\partial_i \tilde{\tau}) + \frac{1}{2} (\partial_i h) (\partial_i h) + U(\tilde{\tau}, h) \right], \quad (20)$$

where $U(\tilde{\tau}, h)$ is the potential of $\tilde{\tau}$ and h . We calculate the potential at one loop level for Higgs potential and at tree level for $\tilde{\tau}$ potential. Now the constraint (19) gives the upper bound on $\mathcal{A}_{\tilde{\tau}\tilde{\tau}h^0}$ for a given stau mass which is shown in Fig.5 of Sec. 2.2.2, for $m_h = 120$ GeV. When we calculate the bounce, we take straight line path from the false vacuum to the true vacuum in $(\tilde{\tau}, h)$ plane. We checked that the full analysis using two dimensional path changes the result from the straight line approximation by only $\mathcal{O}(1)\%$.

We also have to care about the thermal transition of our vacuum to CCB vacuum in the early stage of the universe [19]. The procedure of calculating the thermal transition rate is similar to that of zero temperature case. We use free energy F instead of euclidian action S_E to calculate the bounce solution $\bar{\phi}$. The thermal transition rate at temperature T per unit volume is given by

$$\Gamma(T)/V \simeq T^4 e^{-F[\bar{\phi}, T]/T}. \quad (21)$$

Since the thermal transition must not occur,

$$\int_{t_i}^{t_f} dt \frac{1}{H(t)^3} (\Gamma(T)/V) \ll 1 \quad (22)$$

must be satisfied, where t_i and t_f are initial and final time respectively, and $H(t)$ is the Hubble constant at each time. In our analysis, the free energy takes the form of

$$F[\tau, h, T] = \int_{-\infty}^{\infty} d^3x \left[\frac{1}{2} (\partial_i \tilde{\tau}) (\partial_i \tilde{\tau}) + \frac{1}{2} (\partial_i h) (\partial_i h) + U(\tilde{\tau}, h) + \delta V_{th}(\tilde{\tau}, h, T) \right], \quad (23)$$

where δV_{th} is the thermal potential calculated by thermal field theory. The thermal potential include the contribution from top quark and gauge bosons of U(1) and SU(2) gauge symmetries in the Standard Model. From the constraint (22), We get the upper bound on $\mathcal{A}_{\tilde{\tau}\tilde{\tau}h^0}$. The resultant upper bound on $\mathcal{A}_{\tilde{\tau}\tilde{\tau}h^0}$ for a given stau mass is also shown in Fig.5.

The upper bound on the $\tilde{\tau}\tilde{\tau}H$ trilinear coupling $\mathcal{A}_{\tilde{\tau}\tilde{\tau}H}$, which is discussed in Sec. 2.2.3, can be obtained in the similar way. The result is shown in Fig. 10 for $m_H = 2m_{\tilde{\tau}}$, where we take account of the Higgs potential at tree level, and the contributions from bottom quark, tau lepton and the gauge bosons of the U(1) and SU(2) gauge symmetries for the thermal potential.

References

- [1] V. Khachatryan *et al.* [CMS Collaboration], JHEP **1103** (2011) 024. [arXiv:1101.1645 [hep-ex]]; G. Aad *et al.* [ATLAS Collaboration], [arXiv:1103.1984 [hep-ex]].
- [2] M. Fujii, M. Ibe and T. Yanagida, Phys. Lett. B **579**, 6 (2004) [arXiv:hep-ph/0310142].
- [3] L. Roszkowski, R. Ruiz de Austri and K. Y. Choi, JHEP **0508** (2005) 080 [arXiv:hep-ph/0408227]; J. Pradler and F. D. Steffen, Phys. Rev. D **75** (2007) 023509 [arXiv:hep-ph/0608344]; K. Y. Choi, L. Roszkowski and R. Ruiz de Austri, JHEP **0804** (2008) 016 [arXiv:0710.3349 [hep-ph]]; F. D. Steffen, Phys. Lett. B **669** (2008) 74 [arXiv:0806.3266 [hep-ph]].
- [4] M. Fukugita, T. Yanagida, Phys. Lett. **B174** (1986) 45.
- [5] W. Buchmuller, R. D. Peccei, T. Yanagida, Ann. Rev. Nucl. Part. Sci. **55**, 311-355 (2005). [hep-ph/0502169]; S. Davidson, E. Nardi, Y. Nir, Phys. Rept. **466**, 105-177 (2008). [arXiv:0802.2962 [hep-ph]].
- [6] M. Endo, K. Hamaguchi and K. Nakaji, JHEP **1011**, 004 (2010) [arXiv:1008.2307 [hep-ph]].

- [7] M. Ratz, K. Schmidt-Hoberg and M. W. Winkler, JCAP **0810**, 026 (2008) [arXiv:0808.0829 [hep-ph]].
- [8] J. Pradler and F. D. Steffen, Nucl. Phys. B **809**, 318 (2009) [arXiv:0808.2462 [hep-ph]].
- [9] T. Moroi, H. Murayama and M. Yamaguchi, Phys. Lett. B **303**, 289 (1993).
- [10] M. Bolz, A. Brandenburg and W. Buchmuller, Nucl. Phys. B **606**, 518 (2001) [Erratum-ibid. B **790**, 336 (2008)] [arXiv:hep-ph/0012052].
- [11] J. Pradler and F. D. Steffen, Phys. Lett. B **648**, 224 (2007) [arXiv:hep-ph/0612291].
- [12] V. S. Rychkov, A. Strumia, Phys. Rev. **D75**, 075011 (2007). [hep-ph/0701104].
- [13] M. Endo, F. Takahashi and T. T. Yanagida, Phys. Rev. D **76** (2007) 083509 [arXiv:0706.0986 [hep-ph]], and references therein.
- [14] M. Endo, K. Hamaguchi and F. Takahashi, Phys. Rev. Lett. **96**, 211301 (2006) [arXiv:hep-ph/0602061]; S. Nakamura, M. Yamaguchi, Phys. Lett. **B638** (2006) 389-395. [hep-ph/0602081].
- [15] C. Amsler *et al.* [Particle Data Group], Phys. Lett. B **667** (2008) 1.
- [16] M. Pospelov, Phys. Rev. Lett. **98**, 231301 (2007) [arXiv:hep-ph/0605215]; M. Kamimura, Y. Kino, E. Hiyama, Prog. Theor. Phys. **121** (2009) 1059-1098. [arXiv:0809.4772 [nucl-th]], and references therein.
- [17] M. Kawasaki, K. Kohri, T. Moroi and A. Yotsuyanagi, Phys. Rev. D **78**, 065011 (2008) [arXiv:0804.3745 [hep-ph]], and references therein.
- [18] T. Asaka, K. Hamaguchi and K. Suzuki, Phys. Lett. B **490**, 136 (2000) [arXiv:hep-ph/0005136].
- [19] A. Kusenko, P. Langacker and G. Segre, Phys. Rev. D **54**, 5824 (1996) [arXiv:hep-ph/9602414].
- [20] S. R. Coleman, Phys. Rev. D **15**, 2929 (1977) [Erratum-ibid. D **16**, 1248 (1977)]; C. G. Callan and S. R. Coleman, Phys. Rev. D **16**, 1762 (1977).
- [21] L. Roszkowski, R. Ruiz de Austri and K. Y. Choi, JHEP **0508**, 080 (2005) [arXiv:hep-ph/0408227]
- [22] G. Belanger, F. Boudjema, P. Brun, A. Pukhov, S. Rosier-Lees, P. Salati, A. Semenov, Comput. Phys. Commun. **182**, 842-856 (2011). [arXiv:1004.1092 [hep-ph]].
- [23] See, for instance, L. Roszkowski, R. Ruiz de Austri and K. Y. Choi, in [3] and references therein.

- [24] T. Sjostrand, S. Mrenna and P. Z. Skands, JHEP **0605**, 026 (2006) [arXiv:hep-ph/0603175].
- [25] W. Beenakker, R. Hopker and M. Spira, arXiv:hep-ph/9611232.
- [26] The information on Pretty Good Simulation of high energy collisions (PGS4) can be seen in <http://www.physics.ucdavis.edu/%7Econway/research/research.html>.
- [27] T. Aaltonen *et al.* [CDF Collaboration], Phys. Rev. Lett. **103**, 021802 (2009) [arXiv:0902.1266 [hep-ex]].
- [28] V. M. Abazov *et al.* [D0 Collaboration], Phys. Rev. Lett. **102**, 161802 (2009) [arXiv:0809.4472 [hep-ex]].
- [29] G. Aad *et al.* [The ATLAS Collaboration], arXiv:0901.0512 [hep-ex].
- [30] S. Tarem, S. Bressler, H. Nomoto and A. Di Mattia, Eur. Phys. J. C **62**, 281 (2009).